J. Fluid Mech. (1989), *vol.* 202, *pp.* 515–541
Printed in Great Britain

The linear stability of viscous compressible plane Couette flow

By W. GLATZEL

Max-Planck-Institut für Astrophysik, Karl-Schwarzschild-Straße 1, D-8046 Garching bei München, FRG

(Received 23 May 1988 and in revised form 1 November 1988)

The structure of normal modes in viscous compressible plane Couette flow is investigated. The spectrum is found to consist of two types of modes: the viscous modes, which obtain finite phase velocities by the mechanism of mode pairing; and the sonic modes, whose phase velocity becomes distorted in the supersonic regime. This leads to mode crossings which unfold, depending on the type of crossing modes, either into purely sonic or viscous–sonic instability bands. The latter provide a new example for viscous instability. Both mode pairing of viscous modes and distortion of the phase velocity of sonic modes is caused by the shear. Critical Reynolds numbers for the instabilities are derived.

1. Introduction

The stability of plane Couette flow is a standard problem in fluid mechanics and has been investigated by many authors. An excellent summary of the results obtained so far is given in Drazin & Reid (1981). While viscous incompressible Couette flow has been studied in great detail and seems to be stable (Gallagher & Mercer 1962, 1964 and Gallagher 1974), only a few authors have studied the effect of compressibility on the stability of shear flows in the context of fluid mechanics (see Blumen, Drazin & Billings 1975; Drazin & Davey 1977 and references given there).

The compressibility of matter may certainly be neglected in subsonic flows but must be taken into account when considering supersonic flows. Such flows occur in various astrophysical situations, e.g. in accretion disks, in the solar wind and at the boundaries of galactic and extragalactic jets. In this context the stability of compressible supersonic shear flows has recently become of great interest, since a variety of instabilities have been found (see e.g. Drury 1985; Papaloizou & Pringle 1984, 1985, 1987; Goldreich, Goodman & Narayan 1986; Narayan, Goldreich & Goodman 1987 and Ray 1982). These sonic instabilities already occur in the simplest case of inviscid supersonic plane Couette flow, which has been studied in detail by Glatzel (1988).

In all investigations done so far either viscous incompressible or inviscid compressible flows have been considered. The combined effect of viscosity and compressibility on the stability of a shear flow is still an open question and will be studied in this paper for the simplest case of plane Couette flow.

For sufficiently small Reynolds numbers viscosity has a stabilizing effect and we expect the sonic instabilities occurring in the inviscid flow to become damped, where the determination of the critical Reynolds number at which marginal stability is reached is of particular interest. This is the main motivation for studying the viscous

flow and will be done in §§6 and 7. In §§2–5 we shall derive the relevant equations for this purpose and discuss the modifications of the modal structure due to viscosity as compared with the inviscid flow.

Although viscosity stabilizes at sufficiently small Reynolds numbers, there are situations (e.g. plane Poiseulle flow) where it leads to an instability at high Reynolds numbers and we have speculated in an earlier paper (Glatzel 1987*b*) that some kind of viscous instability might occur in viscous compressible shear flows too. In discussing the modal structure we shall therefore be particularly interested in how such an instability is generated, provided it exists.

2. Basic equations

2.1. *The stationary flow*

We consider a plane shear layer where the velocity $\bar{V}$ is taken in the x-direction and varies linearly with z ($\bar{V} = z$) from $z = -1$ to $z = +1$. Lengths and velocities are measured respectively in units of half of the thickness of the shear layer and the flow speed at the edge of the shear layer. Sound speed a_0, density $\bar{\rho}$ and pressure $\bar{p}$ are taken to be constant and the Mach number M is defined as the ratio of the flow speed at the edge of the shear layer ($z = +1$) and the sound velocity. For simplicity we assume that both the dynamical shear viscosity η and the volume viscosity ζ are constant within the flow and for convenience we define three Reynolds numbers by

$$Re_\nu = \frac{z_0 \bar{V}_0 \bar{\rho}}{\eta}, \tag{2.1}$$

$$Re_\mu = \frac{z_0 \bar{V}_0 \bar{\rho}}{\zeta + \frac{1}{3}\eta}, \tag{2.2}$$

$$\frac{1}{Re_{\mu\nu}} = \frac{1}{Re_\mu} + \frac{1}{Re_\nu}, \tag{2.3}$$

where z_0 and $\bar{V}_0$ are respectively the half-thickness of the shear layer and the velocity at the edge of the shear layer. Rigid boundary conditions are assumed at $z = \pm 1$, which can take up any normal and shear stress but require the velocity of the flow to be equal to the velocity of the boundary at the boundary's position.

2.2. *The equations governing small deviations from the stationary flow*

A flow with the properties given in §2.1 corresponds to an exact solution of the Navier–Stokes equation. Its linear stability will be considered in the following, where the supersonic regime is of particular interest. The relation between the pressure perturbation $\tilde{p}$ and the density perturbation $\tilde{\rho}$ is given by

$$\tilde{p} = a_0^2 \tilde{\rho}, \tag{2.4}$$

where a_0 denotes the adiabatic or isothermal sound velocity. Momentum and continuity equations are linearized in the usual way and, owing to the symmetries of the problem, the perturbations are taken to be proportional to $\exp[\mathrm{i}k(\omega t + x + (k_y/k)\, y)]$. Denoting the perturbed velocity by $\boldsymbol{v}$ and defining

$$\bar{\sigma} = \omega + \bar{V} \tag{2.5}$$

we find

$$\mathrm{i}k\bar{\sigma}\tilde{\rho} + \bar{\rho}\nabla \cdot \boldsymbol{v} = 0, \tag{2.6}$$

$$\mathrm{i}k\bar{\sigma}v_x + v_z \frac{\partial \bar{V}}{\partial z} = -\frac{\mathrm{i}k}{\bar{\rho}}\tilde{p} + \frac{1}{Re_\nu}\left(-k^2 - k_y^2 + \frac{\partial^2}{\partial z^2}\right)v_x + \frac{\mathrm{i}k}{Re_\mu}\nabla \cdot \boldsymbol{v}, \tag{2.7}$$

$$\mathrm{i}k\bar{\sigma}v_y = -\frac{\mathrm{i}k_y}{\bar{\rho}}\tilde{p} + \frac{1}{Re_\nu}\left(-k^2 - k_y^2 + \frac{\partial^2}{\partial z^2}\right)v_y + \frac{\mathrm{i}k_y}{Re_\mu}\nabla\cdot\boldsymbol{v}, \tag{2.8}$$

$$\mathrm{i}k\bar{\sigma}v_z = -\frac{1}{\bar{\rho}}\frac{\partial\tilde{p}}{\partial z} + \frac{1}{Re_\nu}\left(-k^2 - k_y^2 + \frac{\partial^2}{\partial z^2}\right)v_z + \frac{1}{Re_\mu}\frac{\partial}{\partial z}(\nabla\cdot\boldsymbol{v}). \tag{2.9}$$

Boundary conditions for the perturbed quantities follow from the requirement that the fluid has to move with the boundary:

$$v_x = v_y = v_z = 0 \quad \text{at} \quad z = \pm 1. \tag{2.10}$$

2.3. *Squire's theorem for viscous compressible flows*

Squire's theorem can be extended to viscous compressible flows by the following transformation:

$$k'^2 = k^2 + k_y^2, \tag{2.11}$$

$$k'v_x' = kv_x + k_y v_y, \tag{2.12}$$

$$\tilde{p}' = \tilde{p}\frac{k'}{k}; \quad \tilde{\rho}' = \tilde{\rho}\frac{k}{k'}; \quad v_z' = v_z, \tag{2.13}$$

$$\omega' = \omega\frac{k'}{k}, \tag{2.14}$$

$$a_0' = a_0\frac{k'}{k}; \quad \frac{1}{Re_\nu'} = \frac{1}{Re_\nu}\frac{k'}{k}; \quad \frac{1}{Re_\mu'} = \frac{1}{Re_\mu}\frac{k'}{k}. \tag{2.15}$$

By this transformation the general three-dimensional problem is equivalent to a two-dimensional one in the primed quantities ($k_y' = v_y' = 0$). In the following we shall therefore consider only two-dimensional perturbations. Equation (2.14) shows that two-dimensional perturbations are the most unstable ones: for each unstable three-dimensional perturbation there exists a more unstable two-dimensional perturbation. However, we emphasize that the Reynolds numbers and the sound velocity, i.e. the Mach number, have to be transformed too, when three-dimensional and two-dimensional perturbations are compared in this way.

2.4. *The perturbation equation*

The perturbation equations for a two-dimensional perturbation having $k_y = v_y = 0$ may be condensed into a single differential equation for the pressure perturbation. Using (2.4)–(2.9) we find

$$\begin{aligned}
&\frac{\partial^4\tilde{p}}{\partial z^4}\left(1 + \frac{\mathrm{i}k\bar{\sigma}M^2}{Re_{\mu\nu}}\right) + \frac{\partial^3\tilde{p}}{\partial z^3}\left(\frac{4\mathrm{i}kM^2}{Re_{\mu\nu}}\right) \\
&\quad + \frac{\partial^2\tilde{p}}{\partial z^2}\left[-k^2 + M^2k^2\bar{\sigma}^2 - \frac{\mathrm{i}k\bar{\sigma}M^2}{Re_{\mu\nu}} - Re_\nu\left(\mathrm{i}k\bar{\sigma} + \frac{k^2}{Re_\nu}\right)\left(1 + \frac{\mathrm{i}k\bar{\sigma}M^2}{Re_{\mu\nu}}\right)\right] \\
&\quad + \frac{\partial\tilde{p}}{\partial z}\left[4M^2k^2\bar{\sigma}^2 - \frac{2\mathrm{i}k^3M^2}{Re_{\mu\nu}} + 2\mathrm{i}kRe_\nu\left(1 + \frac{\mathrm{i}k\bar{\sigma}M^2}{Re_\mu}\right) - Re_\nu\left(\mathrm{i}k\bar{\sigma} + \frac{k^2}{Re_\nu}\right)\frac{2\mathrm{i}kM^2}{Re_{\mu\nu}}\right] \\
&\quad + \tilde{p}\left[2M^2k^2 - 2M^2k^2\frac{Re_\nu}{Re_\mu} + Re_\nu\left(\mathrm{i}k\bar{\sigma} + \frac{k^2}{Re_\nu}\right)\left(k^2 - M^2k^2\bar{\sigma}^2 + \frac{\mathrm{i}k^3\bar{\sigma}M^2}{Re_{\mu\nu}}\right)\right] = 0.
\end{aligned} \tag{2.16}$$

Similarly the boundary conditions (2.10) may be expressed in terms of $\tilde{p}$ and its derivatives:

$$\frac{\partial^2\tilde{p}}{\partial z^2}\left(1+\frac{\mathrm{i}k\bar{\sigma}M^2}{Re_{\mu\nu}}\right)+\frac{\partial\tilde{p}}{\partial z}\left(\frac{2\mathrm{i}kM^2}{Re_{\mu\nu}}\right)+\tilde{p}\left(-k^2+M^2k^2\bar{\sigma}^2-\frac{\mathrm{i}k^3\bar{\sigma}M^2}{Re_{\mu\nu}}\right)=0;\quad z=\pm1, \tag{2.17}$$

$$\frac{\partial^3\tilde{p}}{\partial z^3}\left(1+\frac{\mathrm{i}k\bar{\sigma}M^2}{Re_{\mu\nu}}\right)+\frac{\partial^2\tilde{p}}{\partial z^2}\left(\frac{3\mathrm{i}kM^2}{Re_{\mu\nu}}\right)$$
$$+\frac{\partial\tilde{p}}{\partial z}\left(-k^2+M^2k^2\bar{\sigma}^2-\frac{\mathrm{i}k^3\bar{\sigma}M^2}{Re_{\mu\nu}}\right)+\tilde{p}\left(4M^2k^2\bar{\sigma}-\frac{\mathrm{i}k^3M^2}{Re_{\mu\nu}}\right)=0;\quad z=\pm1. \tag{2.18}$$

If the shear viscosity vanishes ($Re_\nu\to\infty$) we get instead of (2.16)–(2.18) for the perturbation equation

$$\frac{\partial^2\tilde{p}}{\partial z^2}\left[-\mathrm{i}k\bar{\sigma}\left(1+\frac{\mathrm{i}k\bar{\sigma}M^2}{Re_\mu}\right)\right]+\frac{\partial\tilde{p}}{\partial z}(2\mathrm{i}k)+\tilde{p}\left[\mathrm{i}k\bar{\sigma}\left(k^2-M^2k^2\bar{\sigma}^2+\frac{\mathrm{i}k^3\bar{\sigma}M^2}{Re_\mu}\right)-\frac{2k^2M^2}{Re_\mu}\right]=0. \tag{2.19}$$

For zero shear viscosity the tangential components of the flow velocity and the boundary velocity need not be identical any more. In this case the boundary conditions reduce to $v_z=0$ at $z=\pm1$, which may also be written as

$$\frac{\partial\tilde{p}}{\partial z}\left(1+\frac{\mathrm{i}k\bar{\sigma}M^2}{Re_\mu}\right)+\tilde{p}\left(\frac{\mathrm{i}kM^2}{Re_\mu}\right)=0;\quad z=\pm1. \tag{2.20}$$

The perturbation equation (2.16) or (2.19) together with the boundary conditions (2.17) and (2.18) or (2.20) poses an eigenvalue problem for the complex pattern speed ω which is solved numerically using a Riccati method (details are given in the Appendix). Its solutions will be discussed in the following sections.

2.5. *Singularities of the perturbation equation*

The perturbation equation (2.19) for vanishing shear viscosity has two singularities for $\bar{\sigma}=0$ and $1+\mathrm{i}k\bar{\sigma}M^2/Re_\mu=0$, whereas the perturbation equation (2.16) for the general case has only one singularity for $1+\mathrm{i}k\bar{\sigma}M^2/Re_{\mu\nu}=0$. Owing to these singularities the solution of the eigenvalue problem depends on the choice of the integration path in the complex plane used for the integration of (2.16) and (2.19).

The correct integration path can be obtained by considering the initial-value problem associated with the perturbation equations and applying to them a Laplace transform with respect to time (see Case 1961 and Lin 1961 or Glatzel 1987*a*). The Laplace transform formalism then yields Landau's (1946) prescription for the integration path which has been used for the solution of the eigenvalue problem: the integration path from $z=-1$ to $z=+1$ in the complex plane has to pass any singularity – in our normalization – below the singularity. For growing modes the integration path can always be taken along the real axis.

Associated with each of the singularities is a continuous spectrum. The singularity of (2.19) for $\bar{\sigma}=0$ corresponds to the inviscid incompressible continuum which disappears for finite shear viscosity. The second singularity for $1+\mathrm{i}k\bar{\sigma}M^2/Re_{\mu(\nu)}=0$ is associated with a viscous compressible continuum which disappears for zero viscosity or for an incompressible flow ($M=0$). Accordingly, only the spectrum of a medium at rest and of a viscous incompressible flow is entirely discrete. The latter

is consistent with the fact that the spectrum of the Orr–Sommerfeld problem is discrete (cf. Drazin & Reid 1981) to which (2.16)–(2.18) reduce in the incompressible limit and after a transformation of the dependent variable. In the following we shall restrict ourselves to a detailed discussion of the discrete spectrum only.

3. The limit of low Mach numbers

3.1. *Medium at rest*

One way of realizing the limit of low Mach numbers ($M \to 0$) physically is to keep the sound velocity fixed and to decrease the flow velocity. The limit $M \to 0$ then corresponds to a (viscous) compressible medium at rest. Perturbation equations and boundary conditions for this case are found from (2.4)–(2.10) with $\bar{V} = 0$:

$$\frac{\partial^2(\tilde{p}/\bar{\rho})}{\partial z^2}\left(1+\frac{\mathrm{i}k\omega M^2}{Re_{\mu\nu}}\right)+(\tilde{p}/\bar{\rho})\left(-k^2+M^2k^2\omega^2-\frac{\mathrm{i}k^3\omega M^2}{Re_{\mu\nu}}\right)=0, \tag{3.1}$$

$$\frac{1}{Re_\nu}\frac{\partial^2 v_z}{\partial z^2}-\left(\mathrm{i}k\omega+\frac{k^2}{Re_\nu}\right)v_z=\left(1+\frac{\mathrm{i}k\omega M^2}{Re_\mu}\right)\frac{\partial(\tilde{p}/\bar{\rho})}{\partial z}, \tag{3.2}$$

with

$$v_z=0, \quad \frac{\partial v_z}{\partial z}+\mathrm{i}k\omega M^2(\tilde{p}/\bar{\rho})=0 \quad \text{at} \quad z=\pm 1. \tag{3.3}$$

Equation (3.1) is still valid for $\mathrm{Re}_\nu \to \infty$ whereas (3.2) then determines v_z by a differentiation of the solution of (3.1). In this limit the boundary conditions reduce to $v_z = 0$ at $z = \pm 1$, which is equivalent to $\partial(\tilde{p}/\bar{\rho})/\partial z = 0$ at $z = \pm 1$ (see also §2.4).

In a medium at rest a physically meaningful definition of Mach and Reynolds numbers is not possible. Therefore the Mach and Reynolds numbers occurring in this Section have to be regarded as the suitably normalized inverse of the sound velocity and the viscosity respectively. The reason to keep the definition of Mach and Reynolds numbers is to enable a direct comparison between the medium at rest and the compressible viscous shear flow.

The solution of the perturbation equations (3.1) and (3.2) can be given analytically as a superposition of exponential functions, where the integation constants and the dispersion relation for ω are determined by the boundary conditions. For $Re_\nu \to \infty$ we obtain the dispersion relation

$$\omega M = \pm\left[1+\tfrac{1}{4}\pi^2\frac{n_\mathrm{p}^2}{k^2}-\frac{1}{4}\frac{k^2M^2}{Re_\mu^2}\left(1+\frac{\pi^2}{4}\frac{n_\mathrm{p}^2}{k^2}\right)^2\right]^{\frac{1}{2}} + \frac{1}{2}\frac{\mathrm{i}kM}{Re_\mu}\left(1+\tfrac{1}{4}\pi^2\frac{n_\mathrm{p}^2}{k^2}\right); \quad n_\mathrm{p}=0,\pm1,\pm2,\ldots. \tag{3.4}$$

The dispersion relation (3.4) describes a twofold infinite set of modes which are damped by viscosity. If the viscosity vanishes these modes are identical with the neutrally stable standing sound waves of the system as discussed in an earlier paper (Glatzel 1988). For zero Mach number, which corresponds to infinite sound velocity or incompressibility, the discrete spectrum is empty, since an incompressible medium cannot support internal waves and edge waves are excluded by the boundary conditions. Therefore the modes given by (3.4) are the standing sound waves of the system which are damped by viscosity. No further modes are introduced by a finite viscosity.

For finite Re_ν and Re_μ we find the dispersion relation

$$\left(\frac{\alpha\beta}{k^2}+1\right)^2(e^{2\beta}-e^{2\alpha})^2=\left(\frac{\alpha\beta}{k^2}-1\right)^2(e^{2(\beta+\alpha)}-1)^2, \tag{3.5}$$

with

$$\alpha^2=k^2\frac{1-M^2\omega^2+ik\omega M^2/Re_{\mu\nu}}{1+ik\omega M^2/Re_{\mu\nu}} \tag{3.6}$$

and

$$\beta^2=k^2(1+i\omega Re_\nu/k). \tag{3.7}$$

In general the dispersion relation (3.5)–(3.7) has to be solved for ω numerically. However, more physical insight is gained from explicit approximate solutions. For $\alpha\beta/k^2\gg 1$ the dispersion relation (3.5) can be split into two separate explicit dispersion relations:

$$\omega M=\pm\left[1+\tfrac{1}{4}\pi^2\frac{n_p^2}{k^2}-\frac{1}{4}\frac{k^2M^2}{Re_{\mu\nu}^2}\left(1+\tfrac{1}{4}\pi^2\frac{n_p^2}{k^2}\right)^2\right]^{\frac{1}{2}}$$
$$+\frac{1}{2}\frac{ikM}{Re_{\mu\nu}}\left(1+\tfrac{1}{4}\pi^2\frac{n_p^2}{k^2}\right);\quad n_p=0,\pm1,\pm2,\ldots. \tag{3.8}$$

and

$$\omega=\frac{ik}{Re_\nu}\left(1+\tfrac{1}{4}\pi^2\frac{n_V^2}{k^2}\right);\quad n_V=\pm2,\pm3,\ldots. \tag{3.9}$$

The eigenvalues given by (3.8) and (3.9) are close to the exact eigenvalues for large values of $|n_p|$ and $|n_V|$. For small $|n_p|$ and $|n_V|$ the agreement becomes worse. In particular, modes corresponding to $n_V=0,\pm1$ do not exist. Furthermore, the approximation (3.8) is not valid for low values of M. In the limit $M\to0$ we find the following behaviour from (3.5)–(3.7) for the type of modes described by the approximation (3.8):

$$\omega M=\omega_0+\omega_1M^{\frac{1}{2}}+O(M), \tag{3.10}$$

with

$$\omega_0^2=1+\tfrac{1}{4}\pi^2\frac{n_p^2}{k^2};\quad n_p=0,\pm1,\pm2,\ldots \tag{3.11}$$

and

$$\omega_1^2=\frac{1}{\omega_0^3}\frac{1}{ikRe_\nu};\quad n_p\neq0, \tag{3.12}$$

$$\omega_1^2=\frac{1}{4}\frac{1}{\omega_0^3}\frac{1}{ikRe_\nu};\quad n_p=0, \tag{3.13}$$

where the sign of ω_1 has to be chosen that corresponds to a damped mode.

The modes described by (3.8) or (3.10)–(3.13) have qualitatively the same behaviour as the modes given by (3.4) discussed above. In particular, they both disappear for $M\to0$, i.e. in the incompressible limit and their inviscid limits are identical. Therefore they are the standing sound waves of the system, which are damped by shear and volume viscosity. The damping by shear viscosity is proportional to $M^{-\frac{1}{2}}$ for $M\to0$ rather than having a finite limit as for pure volume viscosity.

The second part of the spectrum described by (3.9) and consisting of damped non-oscillating modes is independent of the Mach number M and is already present in an incompressible medium. However, these modes disappear for zero shear viscosity ($Re_\nu\to\infty$). Therefore their physical origin is the shear viscosity and we shall call them viscous modes in the following.

3.2. *Incompressible flow*

The second way of realizing the limit of low Mach numbers physically consists of keeping the flow velocity fixed and increasing the sound velocity. Then the limit $M \to 0$ corresponds to a (viscous) incompressible shear flow. Perturbation equation and boundary conditions for this case are given by (2.16)–(2.18) where M is set to zero. For zero shear viscosity the eigenvalue problem becomes identical with the inviscid incompressible problem. It is well known that in this case the discrete spectrum is empty (see Drazin & Reid 1981). Note that all terms involving the volume viscosity disappear for $M = 0$. In addition, the singularity in the perturbation equation is no longer present.

The stability of a viscous incompressible linear shear flow is a standard problem in fluid mechanics and has been studied by many authors (for a review see Drazin & Reid 1981). The perturbation equation for this problem is usually expressed in terms of a stream function as dependent variable and is known as the Orr–Sommerfeld equation. In fact, if we rewrite the perturbation equation (2.16) and the boundary conditions (2.17) and (2.18) for $M = 0$ in terms of a stream function instead of the pressure perturbation $\tilde{p}$ as dependent variable we arrive at the Orr–Sommerfeld equation in its standard form. Therefore the solutions of (2.16)–(2.18) contain the solutions of the Orr–Sommerfeld equation. In particular, the results given in a paper by Gallagher (1974) should be identical with the eigenvalues obtained from (2.16)–(2.18) with $M = 0$.

For later comparison and in order to check our analysis we have redone some of Gallagher's (1974) calculations. Our results are shown in figure 1 where the eigenvalues are plotted as a function of the Reynolds number for $k = 1$. In table 1 we have listed the first eigenvalues for $k = 1$ and $Re_\nu = 10^3$ together with the eigenvalues given by Gallagher (1974). Table 1 and figure 1 show reasonable agreement with Gallagher's results. In addition to the first eigenvalues of the viscous modes of the incompressible shear flow we have listed in table 1 the eigenvalues of the viscous modes of the corresponding medium at rest, both as given by (3.5)–(3.7) and by the approximation (3.9). Equation (3.9) provides an excellent approximation to the exact eigenvalue, in particular for large values of $|n_V|$. Furthermore, for large values of $|n_V|$ or small values of the Reynolds number Re_ν the influence of the shear flow is small compared to the influence of viscosity and may be neglected. Accordingly, in this limit the modal structure of the viscous incompressible shear flow is given by the spectrum of the modes for the medium at rest, which can immediately be verified from table 1. We have used this limiting behaviour to order and identify the viscous modes in the shear flow with their counterparts in the medium at rest. All eigenvalues shown in figure 1 and table 1 are therefore labelled with the value of $|n_V|$ of the corresponding mode given by equation (3.9).

As the influence of the shear flow is increased by an increasing Reynolds number or decreasing $|n_V|$ the non-oscillating damped modes begin to pair, thus forming two oscillating modes travelling in opposite x-directions and having the same damping rate (see figure 1). The order of pairing depends on the wavenumbers k and $|n_V|$ (see also Gallagher 1974). With increasing Reynolds number, paired modes eventually unpair and at even higher Reynolds numbers pair again in a different order. Paired oscillating modes are labelled with the two values of $|n_V|$ of the corresponding non-oscillating unpaired modes. For $Re_\nu \to \infty$ the real parts of the pattern speed ω of the oscillating modes approach ± 1 (see figure 1). At a particular finite value of the Reynolds number Re_ν and $M = 0$ we are thus left with a finite number of paired

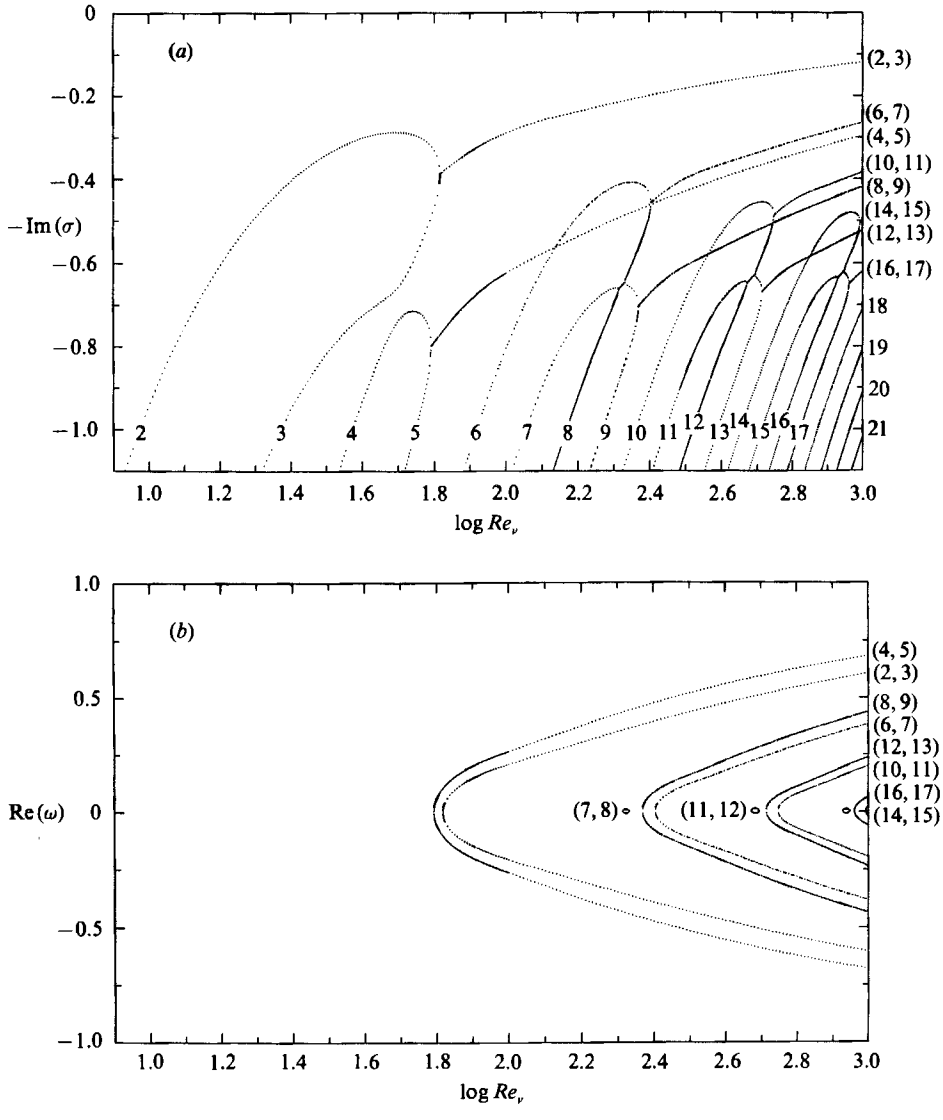

FIGURE 1. (*a*) Damping rates and (*b*) pattern speeds of the viscous modes in the incompressible flow ($M = 0$) for the wavenumber $k = 1$ as a function of the Reynolds number. The curves are labelled with $|n_V|$ or, in the case of pairing, with the values of $|n_V|$ of the two originally unpaired modes.

oscillating and an infinite number of unpaired non-oscillating damped viscous modes (see table 1).

4. The limit of zero viscosity

Perturbation equations and boundary conditions for $Re_\nu \to \infty$ and $Re_\mu \to \infty$ follow directly from (2.19) and (2.20). In this limit the perturbation equation can be solved analytically in terms of confluent hypergeometric functions. A detailed discussion of the properties of the modes in this case may be found in Glatzel (1988) and we shall restrict ourselves to a brief summary of the main results.

Since the vorticity is constant in the flow considered and we have adopted rigid

	Medium at rest		Shear flow			
			This paper		Gallagher (1974)	
$\lvert n_y \rvert$	Approximation Im (ω)	Exact Im (ω)	Re (ω)	Im (ω)	Re (ω)	Im (ω)
40	3.9488	3.9473	0	3.9264	—	—
39	3.7539	3.7513	0	3.7295	—	—
38	3.5639	3.5624	0	3.5393	—	—
37	3.3789	3.3762	0	3.3521	—	—
36	3.1988	3.1972	0	3.1715	—	—
35	3.0236	3.0209	0	2.9940	—	—
34	2.8533	2.8518	0	2.8231	—	—
33	2.6880	2.6854	0	2.6552	—	—
32	2.5276	2.5261	0	2.4938	—	—
31	2.3722	2.3695	0	2.3355	—	—
30	2.2217	2.2201	0	2.1835	—	—
29	2.0761	2.0735	0	2.0348	—	—
28	1.9354	1.9339	0	1.8921	—	—
27	1.7997	1.7971	0	1.7529	—	—
26	1.6690	1.6674	0	1.6193	—	—
25	1.5431	1.5405	0	1.4894	—	—
24	1.4222	1.4207	0	1.3648	—	—
23	1.3063	1.3036	0	1.2441	—	—
22	1.1952	1.1937	0	1.1281	—	—
21	1.0891	1.0865	0	1.0163	—	—
20	0.9880	0.9864	0	0.9087	—	—
19	0.8917	0.8891	0	0.8057	—	—
18	0.8004	0.7989	0	0.7058	—	—
17	0.7141	0.7115	−0.0619	0.6197	—	—
16	0.6327	0.6311	+0.0619	0.6197	—	—
15	0.5562	0.5535	−0.0260	0.4991	—	—
14	0.4846	0.4831	+0.0260	0.4991	—	—
13	0.4180	0.4154	−0.2366	0.5226	—	—
12	0.3563	0.3548	+0.2366	0.5226	—	—
11	0.2996	0.2969	−0.1981	0.3839	—	—
10	0.2477	0.2462	+0.1981	0.3839	—	—
9	0.2009	0.1982	−0.4373	0.4183	—	0.424
8	0.1589	0.1574	+0.4373	0.4183	—	0.424
7	0.1219	0.1193	−0.3838	0.2653	—	0.257
6	0.0898	0.0883	+0.3838	0.2653	—	0.257
5	0.0627	0.0601	−0.6811	0.2962	—	0.301
4	0.0405	0.0389	+0.6811	0.2962	—	0.301
3	0.0232	0.0206	−0.6053	0.1192	—	0.113
2	0.0109	0.0093	+0.6063	0.1192	—	0.113

TABLE 1. The eigenvalues ω of the first viscous modes for $k = 1$, $M = 0$ and $Re_\nu = 10^3$. The second and third column contain the damping rates of the non-oscillating modes in a medium at rest according to the exact dispersion relation (3.5)–(3.7) (column 3) and the approximation (3.9) (column 2), where the order parameter $|n_y|$ occurring in (3.9) is given in column 1. The corresponding eigenvalues of the viscous modes in the shear flow are listed in columns 4 and 5, where the eigenvalues calculated by Gallagher (1974) are shown for comparison in column 5.

boundary conditions the only type of modes that can exist in the inviscid flow are sound waves. For the description of sound waves the appropriate limit of low Mach numbers consists of keeping the sound velocity fixed and decreasing the flow velocity. As described in §3.1 we then obtain for $M \to 0$ a twofold infinite set of standing sound waves travelling in opposite x-directions which are given by (3.4)

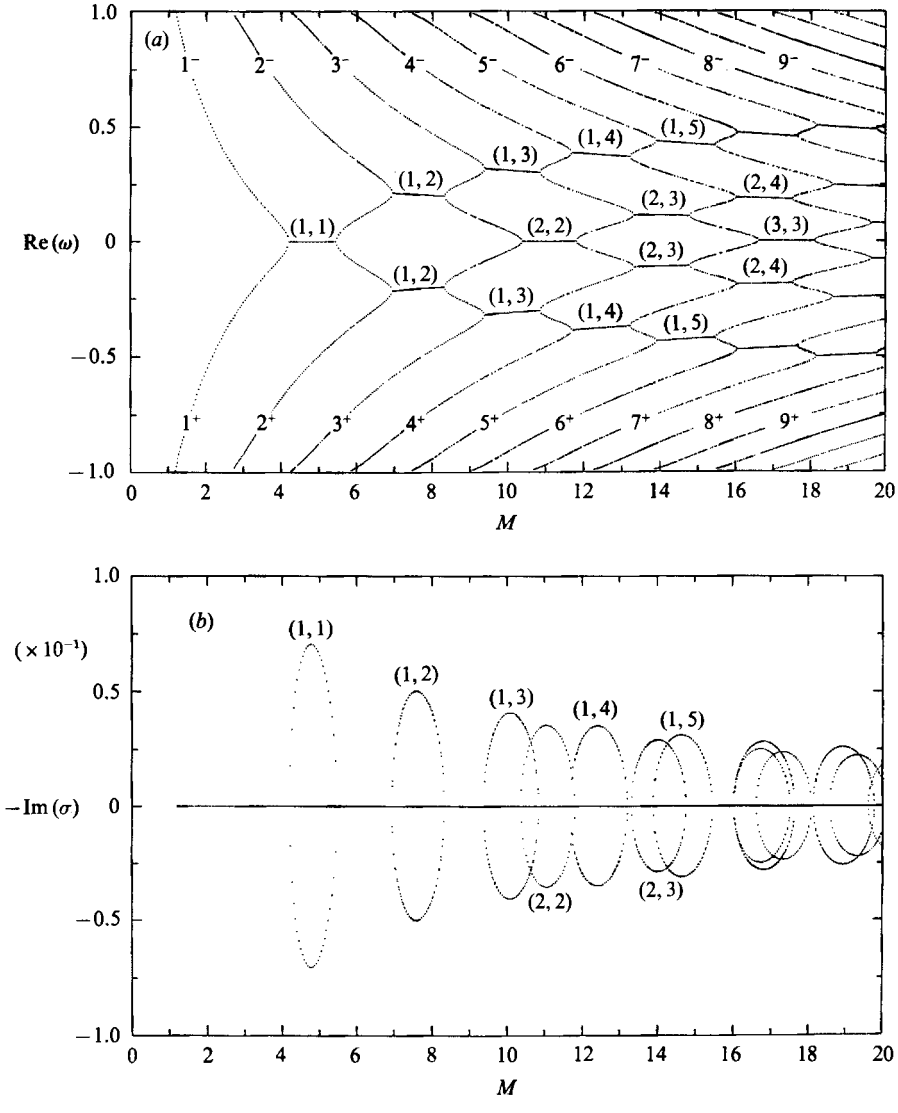

FIGURE 2. (*a*) Pattern speeds and (*b*) growth or damping rates of the sonic modes in the inviscid flow for the wavenumber $k = 1$ as a function of the Mach number. The curves are labelled with $|n_p|+1$, where the sign indicates the x-direction of the wave. Instability bands are labelled with $|n_p|+1$ of the two modes producing the instability by resonance.

with $1/Re_\mu = 0$. Equation (3.4) is still a reasonable approximation to the pattern speed ω for increasing M until the flow speed becomes comparable with the pattern speed of the mode. As the Mach number is increased even more, the pattern speed becomes equal to the flow velocity at some position $|z| \leqslant 1$, i.e. the mode reaches a critical layer within the flow. The shear then causes the pattern speed of the mode to approach the velocity of the boundary moving in the same direction as the mode for $M = 0$. Thereby we obtain mode crossings between the two sets of modes which for $M = 0$ moved in opposite x-directions. These mode crossings unfold into bands of instabilities, i.e. into a pair of complex-conjugate eigenfrequencies. (For the general treatment of mode crossings see Cairns 1979 and Glatzel 1987*a*).

For later comparison with the viscous case we have plotted in figure 2 the real part of the pattern speed ω and the imaginary part of the eigenfrequency $\sigma = \omega k$ for $k = 1$ as a function of the Mach number M. Except for the instability bands all modes are neutrally stable. For $|\mathrm{Re}\,(\omega)| > 1$, i.e. if the mode does not have a critical layer within the flow, ω is approximately given by (3.4) with $1/Re_\mu = 0$. Accordingly we have labelled the modes in figure 2 with $|n_p|+1$. Owing to the symmetry of the problem we have for each value of $|n_p|$ two modes (cf. (3.4)) moving in opposite x-directions. (The direction of propagation is indicated by a superscript of the label.) The resonances are labelled with the values of $|n_p|+1$ of the two associated crossing modes. This convention will also be used in the subsequent sections.

5. The modal structure of viscous compressible flow

We have shown in §3.1 that the spectrum for a viscous compressible medium at rest in general consists of two sets of modes: the viscous modes and the sonic modes. Since the vorticity gradient in the flow considered here vanishes and we had to adopt rigid boundary conditions, no further modes are introduced by the flow itself. Therefore the modes found in viscous compressible plane Couette flow either belong to the viscous type or to the sonic type, where pure volume viscosity only allows for sonic modes, since a finite shear viscosity is necessary for the existence of viscous modes.

For simplicity we shall restrict ourselves in the following to the investigation of pure shear ($\zeta = 0$) and pure volume viscosity ($\eta = 0$). The general case is qualitatively merely a superposition of the two extreme cases. In §§5.1 and 5.2 the sonic and the viscous part of the spectrum for $\zeta = 0$ will be studied and in §5.3 their interaction will be discussed. The purely sonic spectrum for $\eta = 0$ is described in §5.4.

5.1. *The sonic modes for* $\zeta = 0$

As long as the pattern speed of a sonic mode is large compared to the flow speed, i.e. for $|\mathrm{Re}\,(\omega)| \gg 1$, the dispersion relation for the modes in the medium at rest (see (3.5)–(3.7) and (3.10)–(3.13)) yields a good approximation for the modes in the flow. This holds in particular for the limit of low Mach numbers and according to (3.10)–(3.13) we expect the damping rate to be proportional to $M^{-\frac{1}{2}}$ for $M \to 0$. The pattern speed, being close to its inviscid value, approaches a finite limit for $M \to 0$ when normalized by the sound velocity instead of by the flow velocity. (Frequencies in the two normalizations differ by a factor M.)

In order to demonstrate this behaviour of the sonic modes in the limit $M \to 0$ explicitly, we have plotted as full lines in figure 3 the eigenfrequencies of the first three sonic modes (notation as in figure 2) for $Re_\nu = 10^3$ ($Re_\mu = 3Re_\nu$) in a medium at rest according to (3.5)–(3.7). (ωM is the pattern speed in units of the sound speed.) Dots represent the eigenfrequencies of the corresponding modes according to the full problem and dashed lines denote the flow velocities at the boundaries. It is particularly obvious in figure 3 that the pattern speed of a mode is approximately given by the pattern speed of the corresponding mode in the medium at rest until it becomes comparable with the flow speed. The shear then distorts the pattern speed of the modes, thus producing mode crossings and bands of instabilities.

In figure 4 we have plotted in a different range growth and damping rates and the pattern speed of the first three modes for $Re_\nu = 10^3$ as a function of the Mach number. For $|\mathrm{Re}\,(\omega)| < 1$ and large Reynolds numbers Re_ν the eigenvalues are close to the inviscid limit (see §4 and figure 2). However, owing to an intrinsic damping by

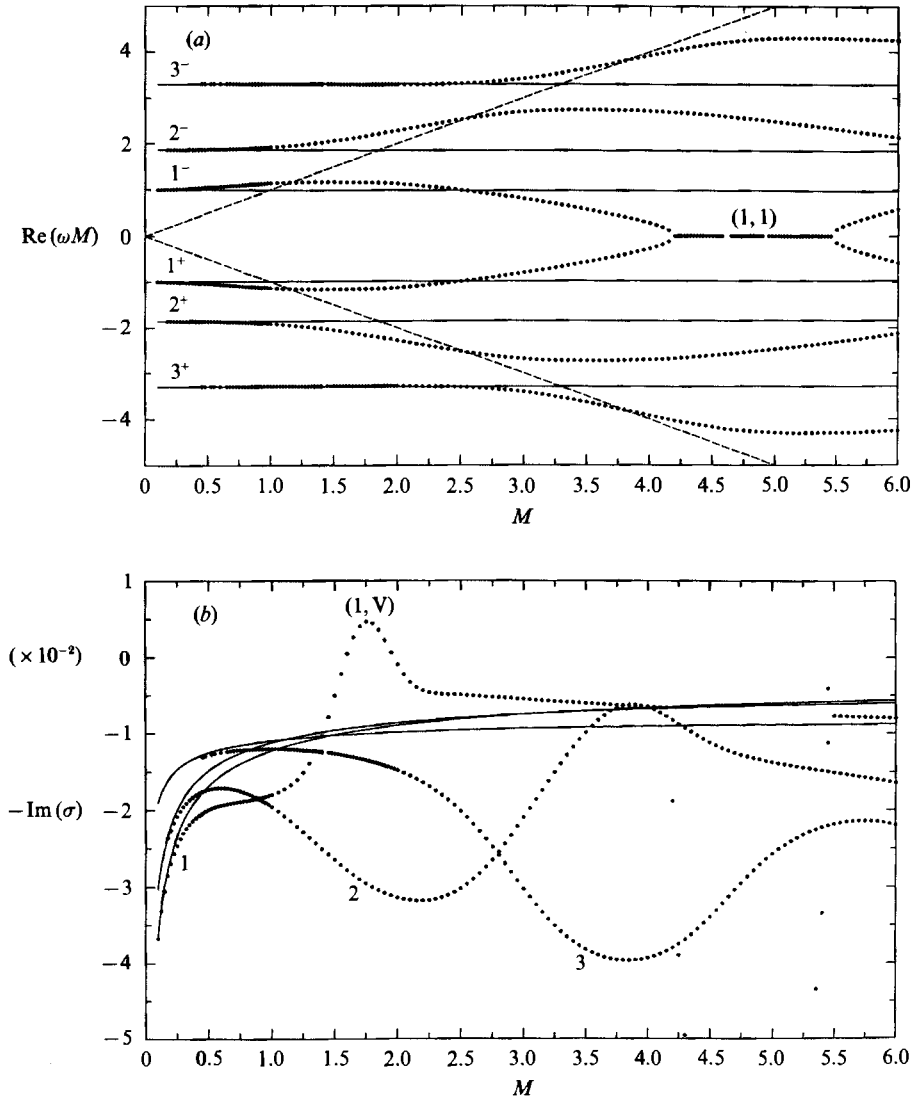

FIGURE 3. (*a*) Pattern speeds in units of the sound velocity and (*b*) growth or damping rates of the first three sonic modes for $k = 1$ and $Re_\nu = 10^3$ ($Re_\mu = 3Re_\nu$) as a function of the Mach number are represented by dots. Full lines show the eigenvalues of the corresponding modes in a medium at rest and dashed lines denote the velocities of the two boundaries of the flow. The curves are labelled as in figure 2. The viscous instability of the sonic mode having $|n_p|+1 = 1$ is denoted by (1, V).

viscosity, modes crossing at $\mathrm{Re}\,(\omega) \neq 0$ do not coincide in the imaginary part of their eigenfrequency and there is no exact crossing of eigenvalues. As a consequence real and imaginary parts of the eigenfrequencies at a crossing having $\mathrm{Re}\,(\omega) \neq 0$ are now uniquely attached to a particular mode.

For a mode corresponding to some value of $|n_p|+1$ the $|n_p|$ crossings denoted by $(n, |n_p|+1)$ having $n < |n_p|+1$ show enhanced damping while crossings with $n > |n_p|+1$ show decreased damping or even instability. The crossing with $n = |n_p|+1$ always occurs at $\mathrm{Re}\,(\omega) = 0$ and is for symmetry reasons an exact crossing. It shows the typical instability band as in the inviscid case. However,

the imaginary parts of the eigenfrequencies are shifted by the intrinsic viscous damping rate of the crossing modes.

The intrinsic damping of the modes by viscosity increases with the Mach number, since the terms involving the viscous damping in (2.19) are proportional to $M^2/Re_{\mu\nu}$. Superimposed on the intrinsic damping rates are the resonance effects as described above.

From figure 4 we find that viscosity has a strong stabilizing influence on the sonic resonance instabilities. At $Re_\nu = 10^3$ the mode with $|n_p|+1 = 3$ is entirely stabilized and the mode having $|n_p|+1 = 2$ shows instability only at the (2, 2) resonance. The exact determination of critical Reynolds numbers for the sonic instabilities will be given in §§6 and 7.

5.2. *The viscous modes for* $\zeta = 0$

Pattern speeds and damping rates of the viscous modes whose incompressible limit was described in §3.2 are plotted as a function of the Mach number for $Re_\nu = 10^3$ in figure 5 (notation as in figure 1). While the non-oscillating modes are almost independent of compressibility, the oscillating viscous modes show a weak dependence and change their order pairwise as the Mach number is increased. This may eventually lead to an unpairing of a mode (see figure 5).

The pairwise changed order of the viscous modes at high Mach numbers is due to a different pairing pattern of the non-oscillating viscous modes when compressibility is important. In figure 6 we have plotted the eigenfrequencies of the viscous modes as a function of the Reynolds number for $k = 1$ and fixed Mach number $M = 10$. Except for the range of very low Reynolds numbers, which will be discussed in the next section, the mode pairing occurs in a much simpler way than in the incompressible case shown in figure 1. The order of modes both in the real and imaginary parts of their eigenvalues is always the same and pairing occurs only between two neighbouring modes.

5.3. *Coupling between sonic and viscous modes* ($\zeta = 0$)

At low Reynolds numbers we have observed in figure 6 a rather complicated modal structure obviously involving not only viscous modes. If we follow the additional modes to higher Reynolds numbers we can identify them with the first three sonic modes. Accordingly the label nS in figure 6 denotes a sonic mode having $|n_p|+1 = n$. The modal structure at low Reynolds numbers in figure 6 may then be explained by a crossing of the (2, 3) viscous mode and the first three sonic modes, where the resonances or crossings give rise to a variety of different types of mode coupling. The ((2, 3); 2S) crossing has unfolded into an ordinary avoided crossing whereas the ((2, 3); 3S) and the (2; 1S) crossings yield much more complicated patterns.

Another type of interaction between sonic and viscous modes occurs at high Reynolds numbers. If we follow the eigenfrequency of a sonic mode (see figures 3 and 4) from zero Mach number, the imaginary part starts to deviate with increasing Mach number from the limit of a medium at rest by reaching a higher damping rate initially. For higher Mach numbers the damping rate decreases again – the higher modes undergo a maximum in the damping rate – and, depending on the Reynolds number and the mode, either a minimum in the damping rate or even an instability is found. These minima or instability bands respectively – labelled (n, V) with $n = |n_p|+1$ – are absent in the inviscid case (figure 2). Accordingly viscosity may be regarded as the origin of this instability. At $Re_\nu = 10^3$ only the mode with $|n_p|+1 = 1$ exhibits the instability while for higher Reynolds numbers the minimum of the damping rate turns into an instability for the higher modes also. Critical Reynolds

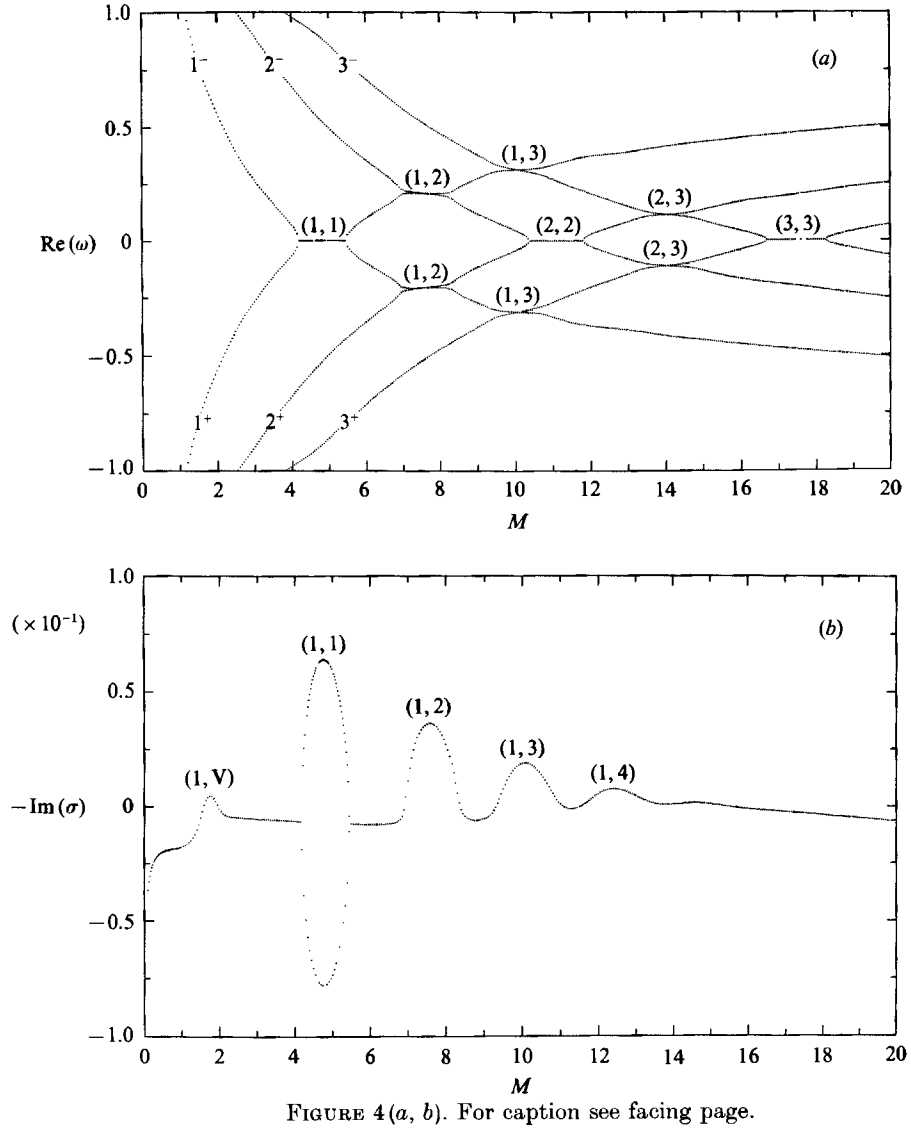

FIGURE 4(*a*, *b*). For caption see facing page.

numbers for these instabilities will be given in §§6 and 7. The modal structure of the sonic modes for even higher Mach numbers has already been described in §5.1.

If we now follow the viscous modes from $M = 0$ we find with increasing Mach number for the two lowest modes denoted by (2, 3) and (4, 5) apart from the general trend several maxima in the damping rate labelled with (n, V) in figure 5. At the position of these maxima, the pattern speed of these modes also seems to be slightly distorted (see figure 5*b* near the label (1, V)). In order to show this behaviour more clearly and to allow for a direct comparison with the relevant sonic modes we have plotted in figure 7 the damping rates of the (2, 3) and the (4, 5) viscous modes on a different scale as a function of the Mach number for $Re_\nu = 10^3$ and $k = 1$.

Since the pattern speed of the oscillating viscous modes always lies within the range of the flow speed and depends only slightly on the Mach number we inevitably get crossings of the pattern speed between the sonic and the viscous modes.

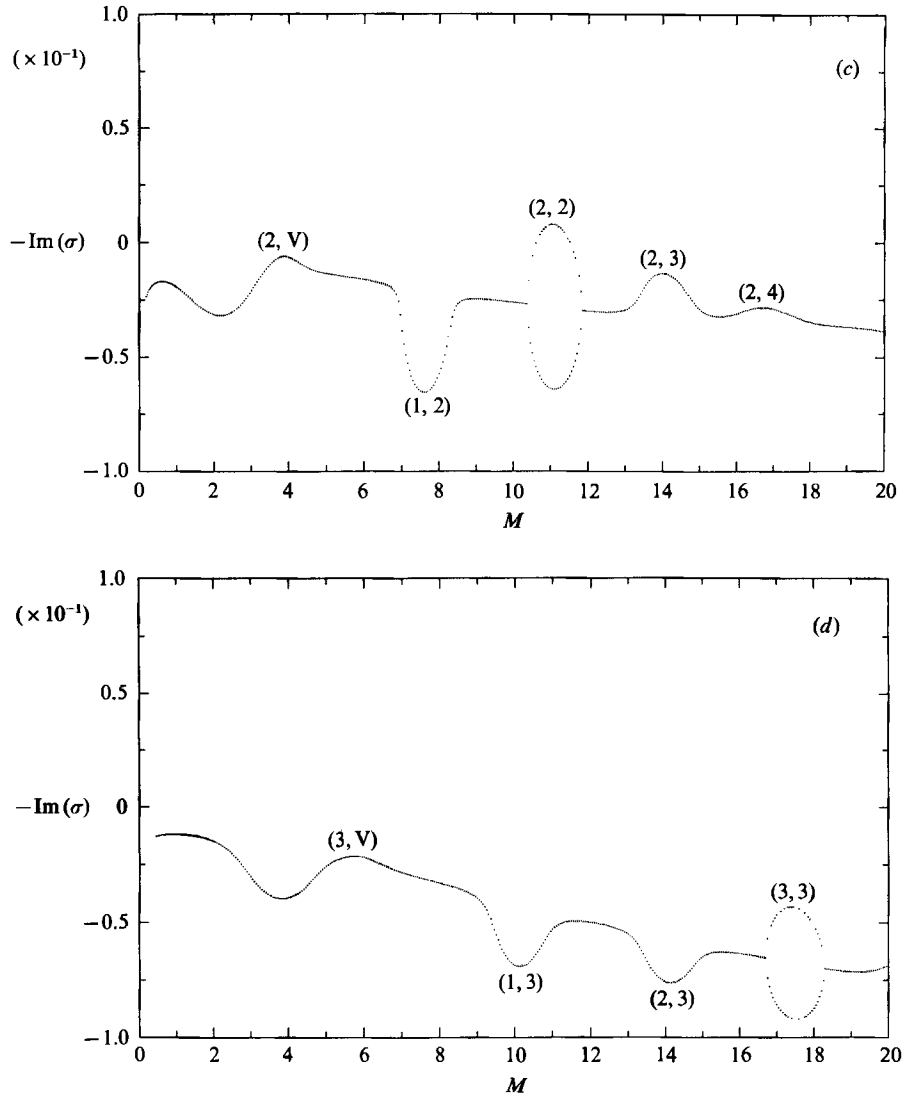

FIGURE 4. Same as figure 2 for the first three sonic modes in a viscous flow having $Re_\nu = 10^3$ ($Re_\mu = 3Re_\nu$). Growth and damping rates of the modes with $|n_p|+1 = 1, 2, 3$ are shown in (b, c, d) respectively. Viscous resonances are denoted by (n, V) with $n = |n_p|+1$.

Comparing figures 4 and 5 we find that the distortion of the pattern speed of the viscous modes (2, 3) and (4, 5) labelled with (1, V) occurs just around their crossing with the sonic mode having $|n_p|+1 = 1$. Furthermore, the maxima in the damping rate of these viscous modes together with the minima in the damping rate or the instabilities of the sonic modes both denoted by (n, V) occur exactly at the Mach number where their pattern speed crosses the pattern speed of the sonic mode with $|n_p|+1 = n$ (see figures 4, 5 and 7).

This phenomenon is explained in a natural way by the resonant interaction of a viscous mode and a sonic mode where the coupling leads to an enhanced damping of the viscous mode and a decreased damping or even a band of instability of the sonic mode. The closer the eigenfrequencies of the crossing viscous and sonic modes are,

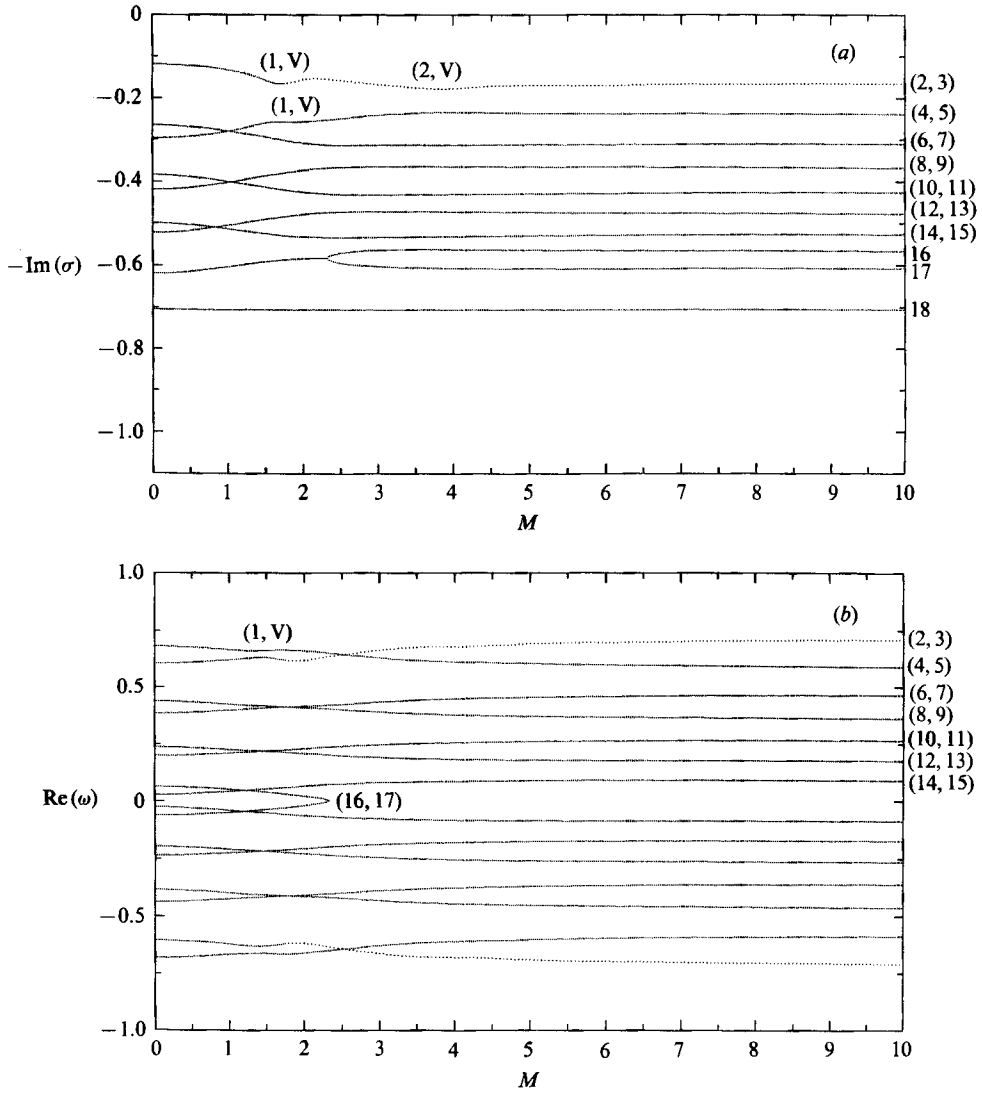

FIGURE 5. (*a*) Damping rates and (*b*) pattern speeds of the first viscous modes for $k = 1$ and $Re_\nu = 10^3$ ($Re_\mu = 3Re_\nu$) as a function of the Mach number. The curves are labelled as in figure 1. The position of resonances with sonic modes having $n = |n_p| + 1$ are denoted by (n, V). Note the unpairing of the mode labelled (16, 17).

the more pronounced is this effect, i.e. for example the viscous mode (2, 3) having the lowest damping rate shows it most clearly (cf. figure 7).

The mechanism of this viscous instability is identical with the mechanism producing the sonic instabilities at infinite Reynolds numbers by resonant interaction of sonic modes and may be interpreted in terms of the energy of a mode, as described in detail in Glatzel (1987*b*). Two modes whose energy has different sign exchange energy by resonant interaction. Thereby the amplitude of both of them can grow without bound, even if the energy of the entire system is to be conserved.

We are thus left with the following details about how viscosity can be responsible for instabilities. Viscosity is the origin of a discrete spectrum of damped modes

having zero pattern speed. The shear causes the modes to pair, thus forming modes with a finite pattern speed, which are still damped. Compressibility provides a spectrum of sound waves, whose pattern speed can coincide with the pattern speed of the paired viscous modes in the supersonic regime. The resonances of paired viscous and sonic modes unfold into bands of instabilities. In this sense viscosity can have a destabilizing effect just by providing a discrete spectrum of modes. Together with a second spectrum of different physical origin, instabilities occur via mode crossings.

5.4. *The sonic modes for* $\eta = 0$

Concerning the viscous damping of the modes at higher Mach numbers, the structure of the sonic resonances and the pattern speed, we find qualitatively the same behaviour as in the case of pure shear viscosity discussed in §5.1 (see figure 4). Plots have therefore been omitted. The only differences to the sonic modes for $\zeta = 0$ occur in the damping rates for low Mach numbers.

In contrast to the case $\zeta = 0$ discussed in §5.1 and plotted in figure 4 the intrinsic damping by viscosity may undergo a minimum as the Mach number decreases and has a finite limit for $M \to 0$. Since the limit $M \to 0$ for the sonic modes corresponds to a medium at rest, these limits of the damping rate should be compared with the damping rates of the corresponding modes in a medium at rest as given by (3.4). In fact, they become identical for $M \to 0$. Owing to zero shear viscosity viscous modes do not exist here and viscous resonances and instabilities do not occur in the sonic modes.

6. Marginal stability

In the previous sections we have studied the modal structure of viscous compressible plane Couette flow. In order to identify the different types of modes and to describe their physical properties it was convenient to discuss the dispersion relations for a fixed perturbation, i.e. for fixed wavenumber k, as a function of the flow properties, i.e. the Mach number M. However, for the determination of critical Reynolds numbers it is more meaningful to consider the stability of a particular flow (fixed M) for various perturbations, i.e. as a function of the wavenumber k.

For the inviscid case it can be verified from analytical approximations that the dispersion relations are symmetric with respect to an interchange of the Mach number M and the wavenumber k (see Glatzel 1988). This symmetry also holds approximately for the exact equations and the viscous flow. Therefore the modal structure as a function of M for fixed k is qualitatively identical with the modal structure as a function of k for fixed M, which is the appropriate basis for the determination of critical Reynolds numbers.

In order to demonstrate this we have plotted in figure 8 pattern speeds and growth rates of the sonic modes in the inviscid flow as a function of the wavenumber for fixed Mach number $M = 20$. Figure 8 should be compared with figure 2. In figure 9 damping and growth rates of the first three sonic modes are shown as a function of k around the viscous–sonic resonances for $M = 4$ and $Re_\nu = 10^5$ ($Re_\mu = 3Re_\nu$). Note the similarity of figure 9 and figure 4. Close to the maximum growth rates in figure 9 we find secondary flat maxima at slightly higher wavenumbers. While the first maxima are caused mainly by resonance with the lowest viscous mode, the secondary maxima are due to resonances with higher viscous modes. Since the strength of a resonance depends on how close the eigenvalues of the modes become at a crossing of their pattern speed, the resonance with the first viscous mode is always the strongest and

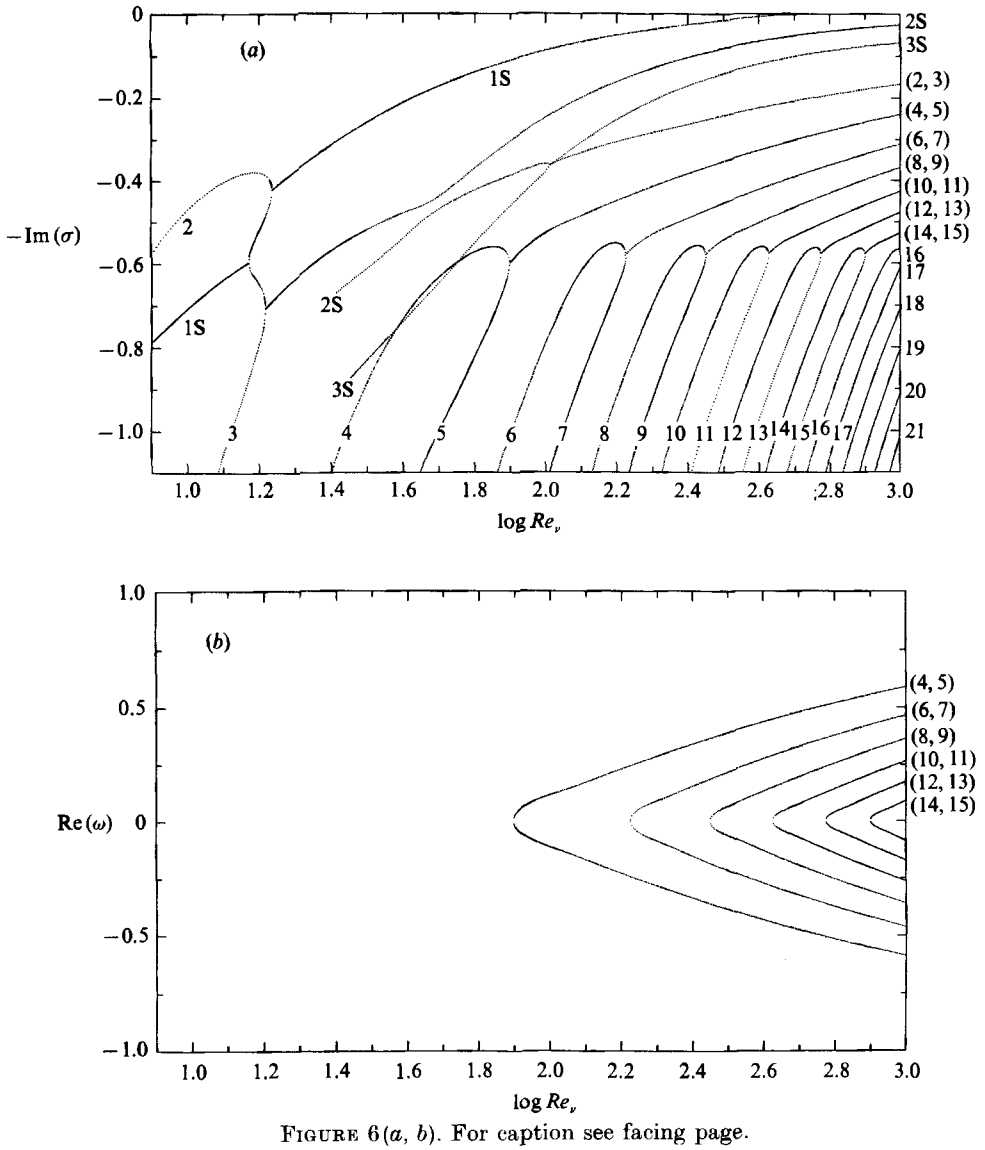

FIGURE 6(*a*, *b*). For caption see facing page.

resonances with higher viscous modes are clearly seen only at very high Reynolds numbers. For the same reason we expect with increasing Reynolds number more and more viscous–sonic resonance instability bands to appear, similar to the multiple resonances of the sonic modes in the inviscid limit.

So far we have determined the complex eigenfrequency ω for given wavenumber k, Mach number M and Reynolds numbers Re_μ and Re_ν by integrating the perturbation equation and iterating ω until the boundary conditions were satisfied. In order to derive critical Reynolds numbers for an instability it is necessary to calculate the Reynolds number where it becomes marginally stable, i.e. where the imaginary part of the eigenfrequency vanishes. Therefore we have to iterate here, instead of the complex eigenfrequency ω, its real part $\mathrm{Re}(\omega)$ and the Reynolds number Re_ν for given k, M and $\mathrm{Im}(\omega) = 0$. In the following we shall for simplicity

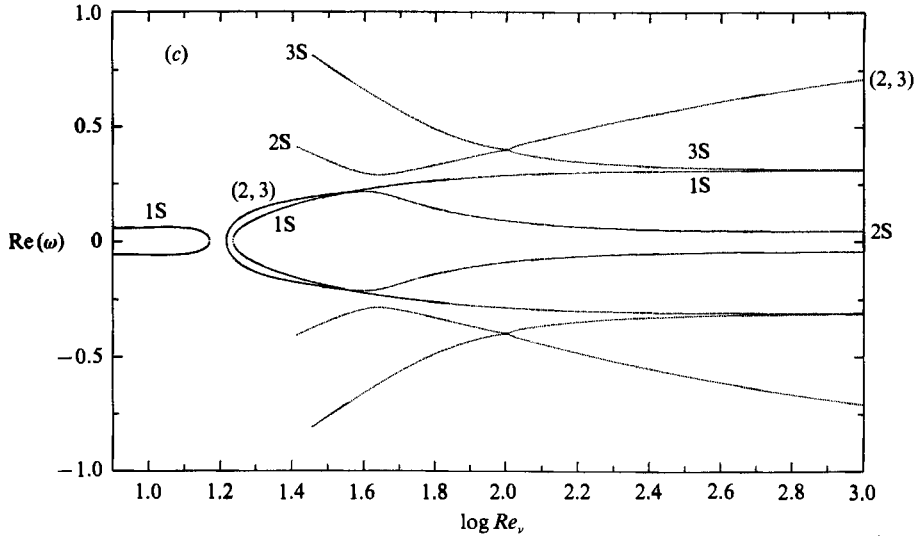

FIGURE 6. Same as figure 1 but for finite compressibility ($M = 10$). Note the different pairing pattern of the viscous modes and the coupling with the first sonic modes labelled nS with $n = |n_p| + 1$.

restrict ourselves to pure shear viscosity, where the two Reynolds numbers are related by $Re_\mu = 3Re_\nu$. For a given flow (fixed M) we then obtain the Reynolds number of marginal stability as a function of the wavenumber k. However, since the instabilities occur in bands, we have to determine for each instability band its curve of marginal stability. These are shown in figure 10 for $M = 20$ and the purely sonic resonances of the first three sonic modes. As the higher instability bands merge, in particular for lower Reynolds numbers, the curve of marginal stability becomes continuous for the higher resonances. For Reynolds numbers below all the curves of marginal stability the flow is stable. If it lies above one of these curves, there is at least one unstable perturbation. The minima of the curves of marginal stability are the critical Reynolds numbers. According to the fact that each instability band has its own curve of marginal stability, we can define a critical Reynolds number for each resonance. These critical Reynolds numbers still depend on the flow parameters, i.e. on the Mach number M.

For the viscous–sonic resonances we can in a similar way define critical Reynolds numbers and calculate curves of marginal stability. These are plotted for $M = 4$ and the first three sonic modes in figure 11 and exhibit a much more complicated structure than those for the purely sonic resonances. In particular, there are wavenumbers where several Reynolds numbers correspond to marginal stability for a given resonance. At low Reynolds numbers this behaviour is reminiscent of the curve of marginal stability for the viscous instability of plane Poiseulle flow (see Drazin & Reid 1981). With increasing Reynolds number the width of the instability strip widens suddenly, due to the instability caused by resonances with the higher viscous modes. The curves of marginal stability separate regions of stability and instability in the (k, Re_ν)-diagram, where the regions enclosed by the curves correspond to instability as indicated in figure 11. We emphasize, however, that the domains of stability and instability refer only to the particular resonances indicated in figures 10 and 11. For a complete picture of the instability of the flow all resonances have to be considered simultaneously.

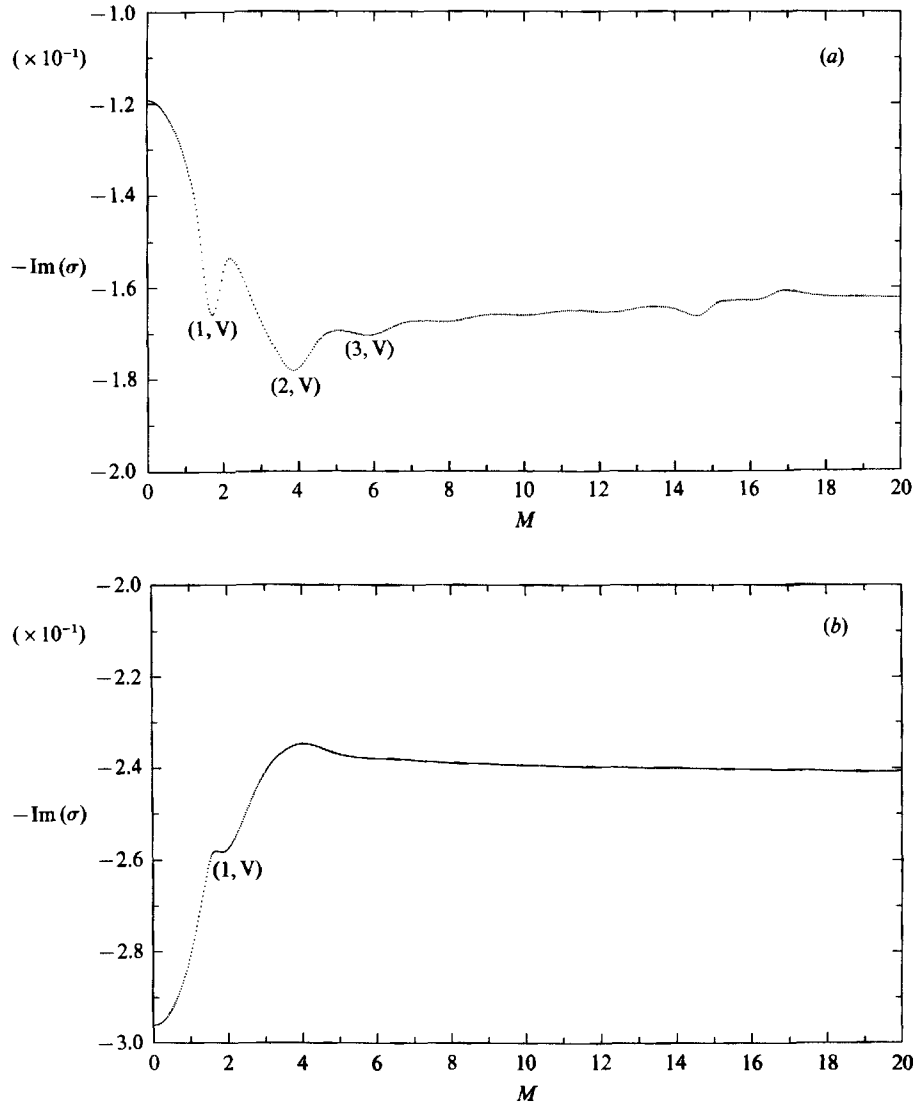

FIGURE 7. The damping rate of (*a*) the (2, 3) viscous mode and (*b*) the (4, 5) viscous mode for $k = 1$ and $Re_\nu = 10^3$ ($Re_\mu = 3Re_\nu$) as a function of the Mach number. Around the resonances with the sonic modes labelled (n, V) $(n = |n_p| + 1)$ local maxima of the damping rate are found.

7. Critical Reynolds numbers

The critical Reynolds number of a particular instability band depends on the flow parameters, i.e. on the Mach number M, and is shown in figure 12 for the resonances indicated. For each instability band the critical Reynolds number has a minimum for some value of M. For higher values the critical Reynolds number increases, since both the growth rates of the instabilities decrease with M and the damping by viscosity is proportional to $M^2/Re_{\mu\nu}$ (see §5.1). The increase for smaller values of M is caused by the fact that the instabilities only exist for supersonic shear velocities. In addition, for an instability band to occur close to sonic velocity one needs high wavenumbers, which imply higher viscous damping and therefore lead to higher

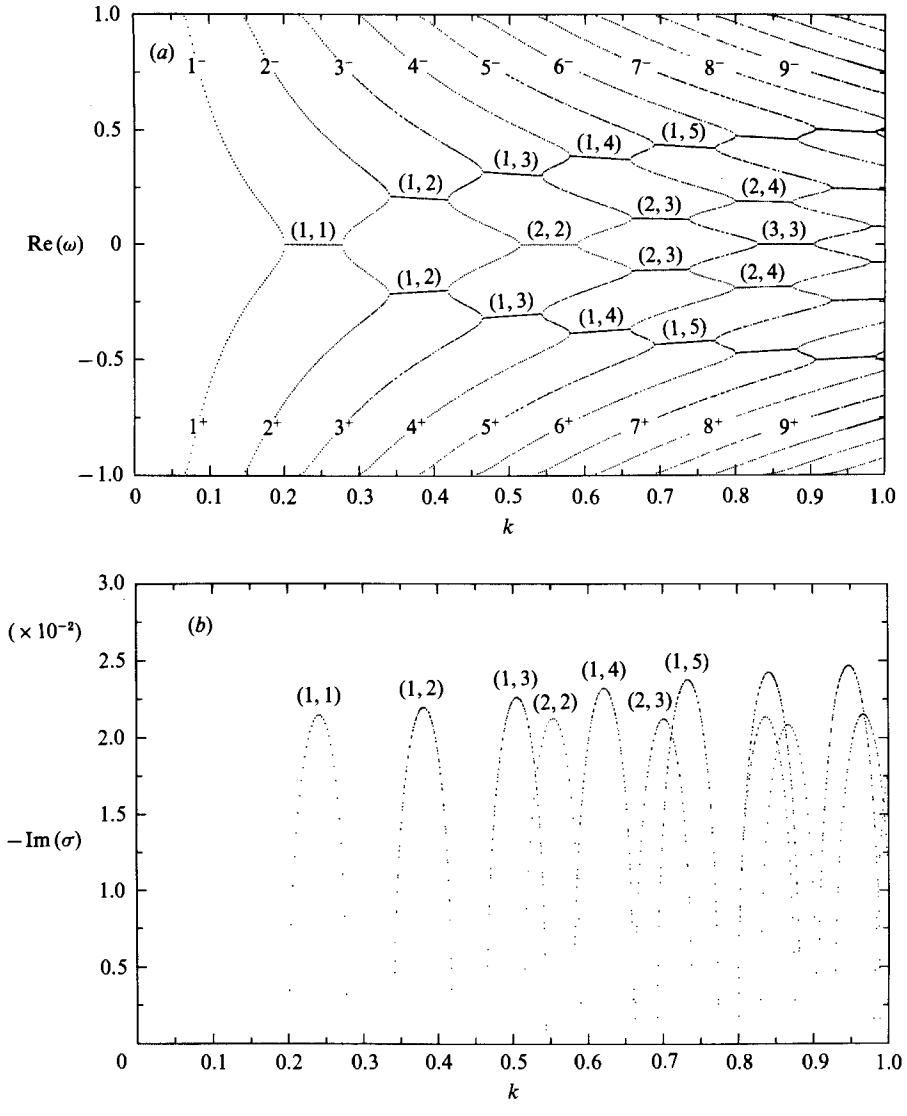

FIGURE 8. (*a*) Pattern speeds and (*b*) growth rates of the sonic modes in the inviscid flow for the Mach number $M = 20$ as a function of the wavenumber. The curves are labelled with $|n_p| + 1$, where the sign indicates the x-direction of the wave. Instability bands are labelled with $|n_p| + 1$ of the two modes producing the instability by resonance.

critical Reynolds numbers. The critical wavenumbers, i.e. the wavenumbers for which the critical Reynolds numbers are attained, are plotted as a function of M in figure 13 for the same resonances as in figure 12.

Basically the critical Reynolds number is determined by two effects: the strength of the instability, i.e. its growth rate in the inviscid limit; and the viscous damping which is proportional to the square of the wavenumber of the perturbation. Therefore the resonances with the higher inviscid growth rates have in general the smaller critical Reynolds numbers. However, the order of the critical Reynolds numbers is not always the same, e.g. the (2, 2) resonance has a smaller critical Reynolds number than the (1, 4) resonance for small Mach numbers and a higher

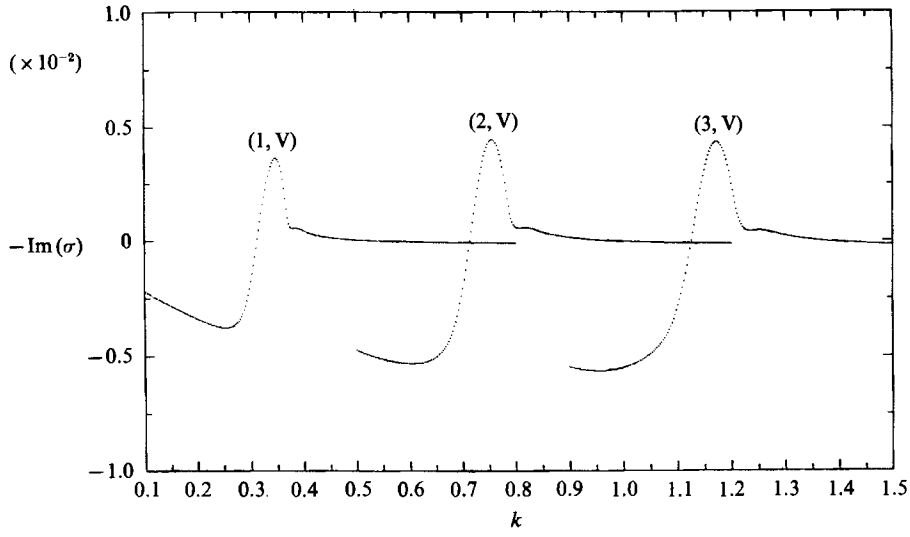

FIGURE 9. Damping and growth rates of the first three sonic modes characterized by $|n_p|+1$ as a function of the wavenumber around the viscous–sonic resonances labelled $(|n_p|+1, \mathrm{V})$ for the Mach number $M = 4$ and the Reynolds number $Re_\nu = 10^5$ $(Re_\mu = 3Re_\nu)$.

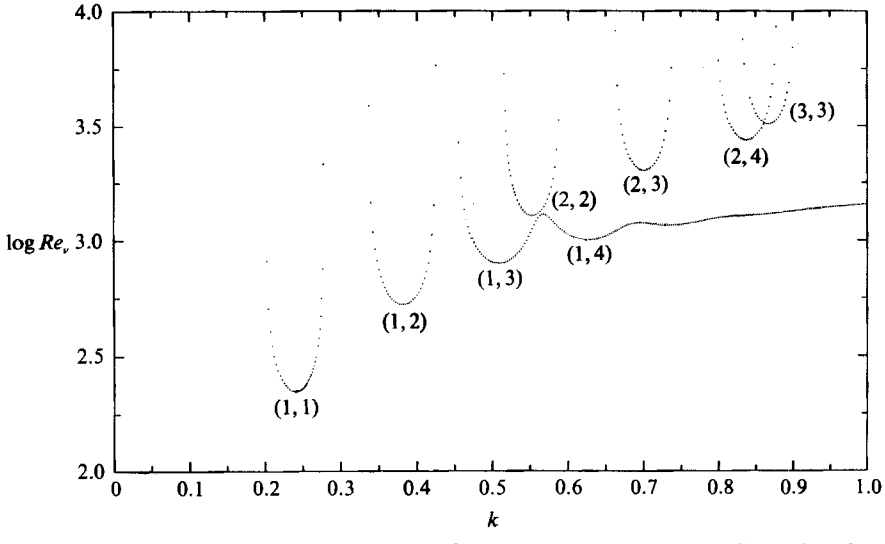

FIGURE 10. Curves of marginal stability for the sonic resonances indicated and the Mach number $M = 20$.

critical Reynolds number for large Mach numbers, which may be interpreted as the competing effects of viscous damping and the strength of the instability. Comparing the purely sonic and the viscous–sonic resonances we find that the sonic resonances (due to higher inviscid growth rates) have lower critical Reynolds numbers for high Mach numbers, whereas for low Mach numbers the viscous–sonic resonances have lower critical Reynolds numbers, which is caused by their lower critical wavenumbers (see figure 13). We note that for a given sonic mode the viscous–sonic resonance always occurs at a lower wavenumber than the sonic resonances. Therefore the minimum critical Reynolds number, below which the flow is stable with respect to

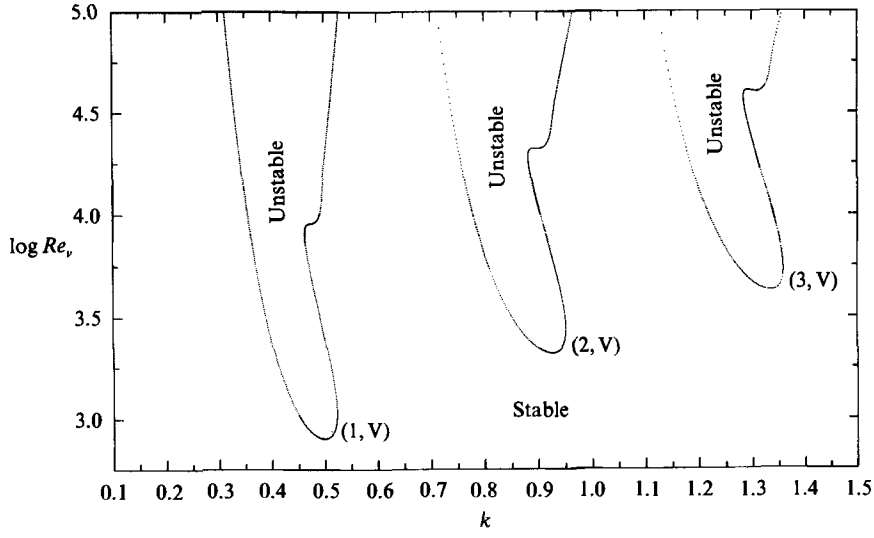

FIGURE 11. Curves of marginal stability for the viscous–sonic resonances indicated and the Mach number $M = 4$.

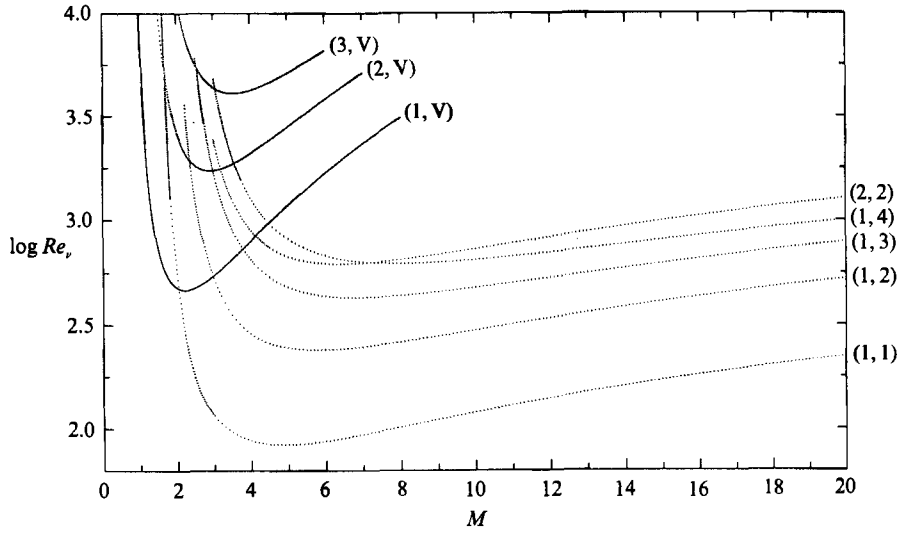

FIGURE 12. Critical Reynolds numbers for the sonic and the viscous–sonic resonance instabilities indicated as a function of the Mach number. Note that the minimum critical Reynolds number is determined by the (1, V) viscous–sonic resonance for low Mach numbers.

all perturbations, is determined by the viscous–sonic (1, V) resonance for low Mach numbers and by the purely sonic (1, 1) resonance for higher Mach numbers (see figure 12). The most unstable flow, i.e. the flow with the lowest minimum critical Reynolds number, has $M = 4.86$. Its minimum critical Reynolds number $Re_\nu = 83.54$ with a critical wavenumber of $k = 0.971$ is given by the (1, 1) resonance.

We emphasize that the critical Reynolds numbers derived here refer to pure shear viscosity ($\zeta = 0$). In general one would have to determine the critical Reynolds numbers including both shear and volume viscosity, i.e. as a function of the ratio $Re_\nu/Re_\mu \geqslant \frac{1}{3}$. However, according to §5.4 a finite volume viscosity has a stabilizing

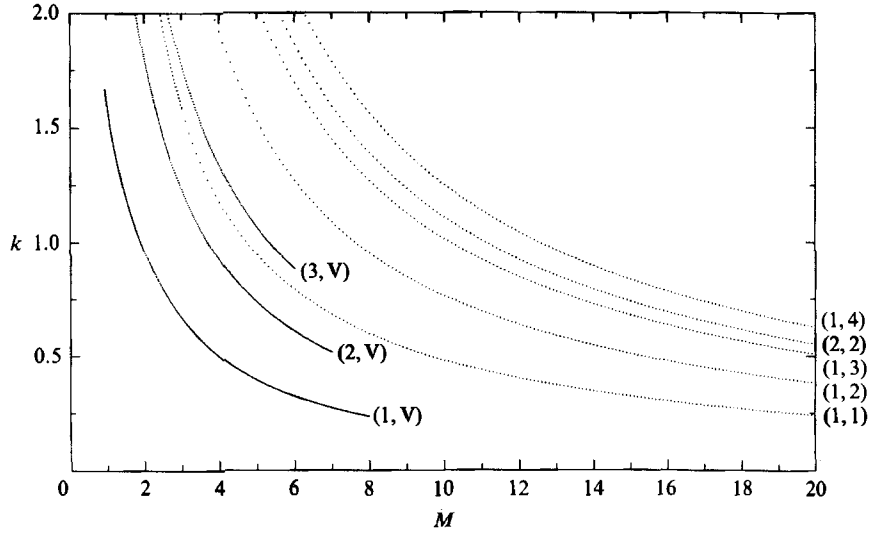

FIGURE 13. Critical wavenumbers for the sonic and the viscous–sonic resonance instabilities indicated as a function of the Mach number.

effect and we expect the amount of shear viscosity necessary to achieve marginal stability to become smaller, i.e. the critical Reynolds numbers Re_ν will increase with increasing Re_ν/Re_μ.

8. Conclusion

We have investigated the modal structure of compressible viscous plane Couette flow. In general the discrete spectrum consists of two sets of modes, which owe their existence to compressibility and viscosity respectively. Both of them can already be found in a medium at rest. If the flow speed is zero, the shear viscosity gives rise to a discrete spectrum of purely damped non-oscillating modes, whereas compressibility provides a discrete spectrum of damped sound waves having a finite pattern speed.

As the flow speed is increased the viscous modes pair, thus attaining a finite pattern speed but still remaining damped, whereas the pattern speed of the sonic modes becomes distorted by the shear. The distortion of the pattern speed of the sonic modes and the effect of mode pairing which gives the viscous modes a finite pattern speed leads to crossings of the pattern speed both among the sonic modes and between the paired viscous and the sonic modes. They always occur in the supersonic regime, since the pattern speed of the sonic modes is supersonic before it becomes distorted for supersonic flow velocities. At all of these resonances or crossings the damping rate of one of the crossing modes is enhanced while the damping of the second is decreased. At high Reynolds numbers the decrease in damping even leads to a band of instability around the resonance.

According to the particular crossing we may distinguish between purely sonic and viscous–sonic resonances. However, the appearance of the resonance and the instability band does not depend on the particular physical nature of the crossing modes. It seems that only the resonance and not any other physical effect is responsible for the instabilities. In this sense the viscous instability at the viscous–sonic resonances is an indirect effect: the role of viscosity is just to provide

an additional discrete spectrum. We suspect that this way of interpreting viscous instabilities may also be viable in other situations. If the instability mechanism is independent of the physical nature of the crossing modes we could imagine that crossings between viscous and vortical or gravity or any other type of modes lead to instability bands in the same way as the crossings of viscous and sonic modes.

Critical Reynolds numbers have been derived for the various instabilities. For low Mach numbers the minimum critical Reynolds number is determined by the first viscous–sonic resonance, and for higher Mach numbers by the first sonic resonance. For $M \to 0$ and $M \to \infty$ the critical Reynolds numbers tend to infinity, where the minimum can be as low as 83.54 at $M = 4.86$ for the first sonic resonance.

Appendix. Numerical solution of the perturbation equation

In order to solve (2.16) with the boundary conditions (2.17) and (2.18) we rewrite it as a system of four first-order equations and introduce new dependent variables u_1, u_2 and v_1, v_2 as

$$u_1 = \frac{\mathrm{i}}{2k}\left[\frac{\partial^2\tilde{p}}{\partial z^2}\left(1+\frac{\mathrm{i}k\bar{\sigma}M^2}{Re_{\mu\nu}}\right)+\frac{\partial\tilde{p}}{\partial z}\left(\frac{2\mathrm{i}kM^2}{Re_{\mu\nu}}\right)+\tilde{p}\left(-k^2+M^2k^2\bar{\sigma}^2-\frac{\mathrm{i}k^3\bar{\sigma}M^2}{Re_{\mu\nu}}\right)\right], \tag{A 1}$$

$$u_2 = \frac{\mathrm{i}}{2k}\left[\frac{\partial^3\tilde{p}}{\partial z^3}\left(1+\frac{\mathrm{i}k\bar{\sigma}M^2}{Re_{\mu\nu}}\right)+\frac{\partial^2\tilde{p}}{\partial z^2}\left(\frac{3\mathrm{i}kM^2}{Re_{\mu\nu}}\right)\right.$$
$$\left.+\frac{\partial\tilde{p}}{\partial z}\left(-k^2+M^2k^2\bar{\sigma}^2-\frac{\mathrm{i}k^3\bar{\sigma}M^2}{Re_{\mu\nu}}\right)+\tilde{p}\left(4M^2k^2\bar{\sigma}-\frac{\mathrm{i}k^3M^2}{Re_{\mu\nu}}\right)\right], \tag{A 2}$$

$$v_1 = \tilde{p}, \tag{A 3}$$

$$v_2 = \frac{\partial\tilde{p}}{\partial z}. \tag{A 4}$$

Defining the vectors $\boldsymbol{u}$ and $\boldsymbol{v}$ as

$$\boldsymbol{u} = \begin{pmatrix} u_1 \\ u_2 \end{pmatrix}; \quad \boldsymbol{v} = \begin{pmatrix} v_1 \\ v_2 \end{pmatrix}, \tag{A 5}$$

and the matrices $\boldsymbol{A}, \boldsymbol{B}, \boldsymbol{C}, \boldsymbol{D}$ as

$$\left.\begin{aligned} \boldsymbol{A} &= \begin{pmatrix} 0 & 1 \\ A_1 & 0 \end{pmatrix}; \quad \boldsymbol{B} = \begin{pmatrix} B_1 & 0 \\ B_2 & B_3 \end{pmatrix}, \\ \boldsymbol{C} &= \begin{pmatrix} 0 & 0 \\ C_1 & 0 \end{pmatrix}; \quad \boldsymbol{D} = \begin{pmatrix} 0 & 1 \\ D_1 & D_2 \end{pmatrix}, \end{aligned}\right\} \tag{A 6}$$

with

$$A_1 = \mathrm{i}k\bar{\sigma}Re_\nu + k^2, \tag{A 7}$$

$$B_1 = -\mathrm{i}k\bar{\sigma}M^2, \tag{A 8}$$

$$B_2 = \mathrm{i}kM^2\left(1+\frac{Re_\nu}{Re_\mu}\right), \tag{A 9}$$

$$B_3 = Re_\nu + \mathrm{i}k\bar{\sigma}M^2\left(1+\frac{Re_\nu}{Re_\mu}\right), \tag{A 10}$$

$$C_1 = \frac{-2\mathrm{i}k}{1+\mathrm{i}k\bar{\sigma}M^2/Re_{\mu\nu}}, \tag{A 11}$$

$$D_1 = \frac{k^2 - k^2M^2\bar{\sigma}^2 + \mathrm{i}k^3\bar{\sigma}M^2/Re_{\mu\nu}}{1 + \mathrm{i}k\bar{\sigma}M^2/Re_{\mu\nu}}, \tag{A 12}$$

$$D_2 = \frac{-2\mathrm{i}kM^2/Re_{\mu\nu}}{1 + \mathrm{i}k\bar{\sigma}M^2/Re_{\mu\nu}}, \tag{A 13}$$

the system of differential equations can be written as

$$\boldsymbol{u}' = \boldsymbol{A}\boldsymbol{u} + \boldsymbol{B}\boldsymbol{v}, \quad \boldsymbol{v}' = \boldsymbol{C}\boldsymbol{u} + \boldsymbol{D}\boldsymbol{v}, \tag{A 14}$$

where a prime denotes differentiation with respect to z and the boundary conditions are given by

$$\boldsymbol{u} = 0; \quad z = \pm 1. \tag{A 15}$$

Since it suffers from the parasitic growth problem (see Drazin & Reid 1981), the numerical solution of the system (A 14) together with the boundary conditions (A 15) using an initial–value method is not possible. However, this difficulty can be overcome by the Riccati method as described by Scott (1973) and Davey (1977). (For a short summary of the method and further references see also Drazin & Reid 1981.) Instead of integrating $\boldsymbol{u}$ and $\boldsymbol{v}$ we solve the differential equation for the (complex) Riccati matrix $\boldsymbol{R}$ defined by

$$\boldsymbol{u} = \boldsymbol{R}\boldsymbol{v} \tag{A 16}$$

From equation (A 14) we find the differential equation for $\boldsymbol{R}$:

$$\boldsymbol{R}' = \boldsymbol{B} + \boldsymbol{A}\boldsymbol{R} - \boldsymbol{R}\boldsymbol{D} - \boldsymbol{R}\boldsymbol{C}\boldsymbol{R}. \tag{A 17}$$

Equation (A 17) is integrated from $z = -1$ to $z = +1$ where the boundary condition (A 15) requires the initial condition (see Davey 1977)

$$\boldsymbol{R} = 0; \quad z = -1, \tag{A 18}$$

and is satisfied at $z = +1$ if $\quad \det \boldsymbol{R} = 0; \quad z = +1. \tag{A 19}$

The condition (A 19) is used to determine the complex pattern speed ω or, for given k, M and $\mathrm{Im}(\omega) = 0$, its real part and the Reynolds number Re_v (see §6). Thus the problem of finding eigenvalues is reduced to the problem of finding the complex zeros of a complex function.

Integration and iteration of (A 17) and (A 19) can be done using any standard routine, e.g. D02CAF and C05NBF from the NAG library. By choosing the error bounds in these routines as small as possible, the eigenvalues could be calculated with a relative accuracy better than 10^{-8}. To check the accuracy of the Riccati method we have also calculated the eigenvalues of the Orr–Sommerfeld problem for incompressible plane Poiseulle flow. A comparison with the very accurate results given by Orszag (1971) which were obtained using Chebyshev expansions showed perfect agreement. The time necessary to calculate an eigenvalue sensitively depends on the parameters and the required accuracy. On the average we needed 1 s per eigenvalue on a CRAY-XMP for a relative accuracy of 10^{-6}.

The Riccati matrix may become singular on the integration path chosen. In this case the path of integration was deformed in the complex plane as suggested by Davey (1977). Occasionally the convergence of the eigenvalue iteration can be considerably accelerated if (A 17) with the initial condition (A 18) is integrated from $z = -1$ and $z = +1$ to some intermediate point, which yields two Riccati matrices. Continuity of the variables then requires the determinant of the difference of the two matrices to vanish, which can be used instead of (A 19) to iterate the eigenvalue.

REFERENCES

BLUMEN, W., DRAZIN, P. G. & BILLINGS, D. 1975 *J. Fluid Mech.* **71**, 305.

CAIRNS, R. A. 1979 *J. Fluid Mech.* **92**, 1.

CASE, K. M. 1961 *J. Fluid Mech.* **10**, 420.

DAVEY, A. 1977 *J. Comp. Phys.* **24**, 331.

DRAZIN, P. G. & DAVEY, A. 1977 *J. Fluid Mech.* **82**, 255.

DRAZIN, P. G. & REID, W. H. 1981 *Hydrodynamic Stability*. Cambridge University Press.

DRURY, L. O'C. 1985 *Mon. Not. R. Astr. Soc.* **217**, 821.

GALLAGHER, A. P. 1974 *J. Fluid Mech.* **65**. 29.

GALLAGHER, A. P. & MERCER, A. McD. 1962 *J. Fluid Mech.* **13**, 91.

GALLAGHER, A. P. & MERCER, A. McD. 1964 *J. Fluid Mech.* **18**, 350.

GLATZEL, W. 1987*a* *Mon. Not. R. Astr. Soc.* **225**, 227.

GLATZEL, W. 1987*b* *Mon. Not. R. Astr. Soc.* **228**, 77.

GLATZEL, W. 1988 *Mon. Not. R. Astr. Soc.* **231**, 795.

GOLDREICH, P., GOODMAN, J. & NARAYAN, R. 1986 *Mon. Not. R. Astr. Soc.* **221**, 339.

LANDAU, L. 1946 *J. Phys. USSR* **10**, 25.

LIN, C. C. 1961 *J. Fluid Mech.* **10**, 430.

NARAYAN, R., GOLDREICH, P. & GOODMAN, J. 1987 *Mon. Not. R. Astr. Soc.* **228**, 1.

ORSZAG, S. A. 1971 *J. Fluid Mech.* **50**, 689.

PAPALOIZOU, J. C. B. & PRINGLE, J. E. 1984 *Mon. Not. R. Astr. Soc.* **208**, 721.

PAPALOIZOU, J. C. B. & PRINGLE, J. E. 1985 *Mon. Not. R. Astr. Soc.* **213**, 799.

PAPALOIZOU, J. C. B. & PRINGLE, J. E. 1987 *Mon. Not. R. Astr. Soc.* **225**, 267.

RAY, T. P. 1982 *Mon. Not. R. Astr. Soc.* **198**, 617.

SCOTT, M. R. 1973 *J. Comp. Phys.* **12**, 334.